Effect of the Electrode Extension on the Geometry of Parts Made of 316LSi Steel by Wire Arc Additive Manufacturing Method

Przemysław Połaski[1], Dariusz Golański[1*], Paweł Kołodziejczak[1], Anna Pakuła[2]

[1] Department of Welding Engineering, Warsaw University of Technology, ul. Narbutta 85, 02-524 Warsaw, Poland

[2] Institute of Micromechanics and Photonics, Warsaw University of Technology, ul. Św. A. Boboli 8, 02-524 Warsaw, Poland

* Corresponding author's email: dariusz.golanski@pw.edu.pl

ABSTRACT

Intensive research is currently being conducted on wire arc additive manufacturing (WAAM) processes. Previous studies have demonstrated the impact of current parameters on altering the structure and properties of 316L stainless steel. However, there is a lack of comprehensive information in the literature regarding the influence of electrode extension length (contact to tube distance) on changes in the structure and geometry of parts made of 316L steel using the cold metal transfer (CMT) method. This parameter was often assumed to be constant in research experiments. The study aimed to determine how the length of the electrode extension affects the geometric properties of steel walls produced in the WAAM CMT additive manufacturing process. The experiment used 316LSi stainless steel to build 3D structures in the shape of straight walls. The chosen shape of the parts yielded the most benefits for preparing samples from the resulting structures for destructive testing. The research demonstrated that the length of the electrode extension is a crucial parameter in the additive manufacturing process of structures using the WAAM method. Modifying the electrode extension length in the WAAM process with a CMT machine impacts the bead geometry and, consequently, the overall model geometry. A 6 mm increase in the electrode extension length resulted in a model that was over 8 mm taller, despite using the same number of layers.

Keywords: wire arc additive manufacturing, cold metal transfer, electrode extension, 316L steel.

INTRODUCTION

Robotization and incremental technologies are at the core of Industry 4.0. The rapid development of specialized 3D solid modeling software is crucial for their advancement. Additive manufacturing, unlike conventional production methods such as machining, plastic forming, and casting, reduces energy and material consumption while maintaining production flexibility [1-2]. In contrast to subtractive methods, where the product is shaped by removing material, additive technologies apply new material to previously produced layers in a successive manner.

Currently, laser-based additive technologies are widely used, including selective laser melting (SLM), selective laser sintering (SLS), laser engineering net shaping (LENS), electron beam melting (EBM), direct energy deposition (DED) as well as plasma welding and thermal spraying [3-4]. New solutions and methods for incrementally producing machine parts include arc welding supported by laser radiation, such as one drop per laser pulse (ODPP) and high-performance cladding with double-wire technology with non-transferred arc and laser-assisted penetration control (HoDopp) technology.

Incremental techniques based on arc surfacing derived directly from the gas metal arc welding (GMAW) methods are not widely known or used. It is important to note that these techniques should be used in conjunction with other welding methods for optimal results. However, they offer several benefits such as the ability to produce

new products or reconstruct damaged and worn parts of a structure. These techniques can also help to reduce production costs and shorten production time. Additive manufacturing by the arc surfacing method (WAAM) offers technological and economic advantages over traditional manufacturing techniques like casting or forging [5]. Among other benefits, additive manufacturing offers the ability to easily adapt the production process to specific requirements, produce complex geometries that are difficult or impossible to achieve with conventional methods, and limit excessive material processing and equipment requirements. This is particularly useful for manufacturing and repairing complex metal elements or large parts [6]. The WAAM technology offers several advantages over other methods of 3D structure additive manufacturing. It significantly reduces the time and cost of manufacturing parts and allows for on-site production using mobile stations. Additionally, the WAAM method enables the production of large and long parts [7].

In recent years, new varieties of arc welding processes, such as CMT, have been introduced. These low-energy welding processes allow for more precise and controlled dosing of material in the electric arc, making them ideal for welding thin sheets [8-9]. As a result, low-energy welding processes have become a promising group of methods for use in additive manufacturing of machine parts and regeneration processes [10]. WAAM technology is an attractive option for regeneration processes as it reduces the time and cost associated with replacing the entire element. This method is particularly useful for regenerating large-size tools used in the mining industry or large-size machine parts with closed geometry that cannot be produced using other additive manufacturing methods [11]. This technology can be used to produce centrifugal impellers for high-performance industrial pumps. The WAAM additive technology can also be used to regenerate railway turnouts. This method is more durable than other 3D printing methods that are subject to wear and tear.

Research on WAAM additive welding has been conducted for various metals and alloys [12]. The most commonly studied group is austenitic stainless steels, which are widely used in modern industries such as aerospace, energy, turbine industries, and chemical production due to their excellent corrosion resistance, high-temperature mechanical properties, and good fabrication

and welding processing abilities [13–15]. The electrode extension is the length of the electrode wire counted from the end of the contact tube. Increasing the electrode extension increases the electrical resistance of the circuit, which in turn increases the amount of heat released and the temperature, resulting in a higher melting rate [16]. The wire electrode is preheated in this area. The size of the weld bead is affected by the length of the electrode extension, which in turn affects the melting rate and depth of penetration. Increasing the electrode extension increases the preheating of the wire and reduces the current intensity, resulting in less penetration in the welded material. For a short arc, the electrode extension is typically between 5–15 mm. When welding stainless steel, lower extension values are more commonly used due to its higher resistance. Conversely, a longer extension is used when using a spray arc and larger electrode diameters [17–19]. Using an excessively long arc in active gases can reduce the mechanical properties of the weld. This is because during the transfer of metal droplets in the arc, various alloying elements burn out. To achieve proper weld quality, it is crucial to determine the correct relationship between electrode extension and current, as well as between penetration depth and electrode extension.

Similar relationships occur in arc processes such as wire electrode surfacing and WAAM processes, where it is essential to control the amount of heat input into the manufactured part to maintain the best possible geometric parameters of the elements. Previous research on producing machine parts using the WAAM method has focused on assessing various factors that can significantly impact the quality and properties of the resulting elements. The key factors include the welding technology parameters (current intensity, voltage, welding speed) [5], the type of welding heat source used (GMAW, plasma, gas tungsten arc welding – GTAW, and their modifications) [7], the trajectory of incremental welding [20], the type and method of cooling the elements after each layer, possible post-surfacing heat treatments [13], or other operations aimed at reducing the level of residual stresses after the surfacing process [14].

The study conducted in [21] examined the impact of different shielding gases on the stability of the arc and the uniformity of the bead produced using stainless steel and creep-resistant steel. Two gases were tested: M12 (98%Ar-2%CO_2) and M14 (96%Ar-3%CO_2-1%O_2). The authors found

that using M14 gas increases penetration at the wall edges, improves mixing, and eliminates the risk of lack of penetration. Additionally, M14 gas improves the flatness of the produced wall. The presence of oxygen enhances the fluidity of the liquid metal and restricts alterations in wall flatness. The effect of the arc voltage and the shielding gas ($Ar+2.5CO_2$, $Ar+20He+2CO_2$) on the structure of the 2209 duplex steel during WAAM processing was investigated in a study [22]. It was found that when changing the parameters, it's important to note that an increase in the voltage leads to a higher specific heat input, which results in a longer cooling time ($\Delta t12/8$) and a higher austenite content. Increasing the proportion of helium in the shielding gas also increases the austenite content.

A study [23] investigated the impact of GTAW welding parameters on the joint strength, hardness, and surface roughness of 316L steel. The research showed that the surface roughness was most affected by the current intensity, the voltage and the flow rate of the shielding gas. The effect of GMAW welding parameters on surface roughness using the additive technique was investigated in [24]. Various parameters were tested, including inter-layer temperature, wire feed speed, travel speed, and the constant ratio of wire feed speed to travel speed. The study found that reducing the interpass temperature can decrease surface wall roughness. It has been demonstrated that increasing the surfacing speed improves surface roughness, but only up to a certain point. Beyond this point, roughness increases due to the arc becoming more unstable at higher speeds.

Work [25] compared the incremental welding of a sleeve made of 308L steel using the CMT and GMAW methods. The study tested the strength, hardness, and microstructure of the produced structures. The results showed that surfacing using the CMT method resulted in higher strength, hardness, and elongation (by approximately 4 to 7%) regardless of the direction in which the test samples were cut. The CMT method reduces heat input and increases cooling rate, resulting in a more fragmented structure, particularly in the lower zones of welded elements. Anisotropy of welded material properties was evident in tests conducted on samples cut in various directions. In [26], a detailed analysis of the anisotropy of 316L steel structures produced through the WAAM method is presented. The study shows that samples cut in the direction of welding exhibit the highest strength, while those cut diagonally (45°) have the highest elongation to failure ratio.

Work [27] investigated the influence of layer stacking direction on the surfacing of WAAM cantilever beams made from 304L steel. Due to the anisotropy of the welded material's properties, optimizing the welding trajectory can lead to significant improvements. The study found that welding directions inclined to the beam axis produced more favorable results than horizontal or vertical directions. The strength of structures produced through the WAAM additive welding process can be further increased by applying heat treatment afterwards. This applies to both the directly aged condition and the solution treated + aged conditions, as demonstrated in the case of 17-4 PH stainless steel [28]. Numerous studies have focused on optimizing the parameters of the incremental welding process [29]. These studies primarily assess the impact of current parameters, heat input, and welding trajectory.

The research summary highlights key factors that affect the welding of incremental WAAM. These include current parameters, heat input [30], gas type, cooling method, welding speed, and wire feed speed (deposition rate) [31]. In addition, high residual stresses can have a significant impact on the durability of the product [32]. The aim of this paper is to investigate the impact of electrode extension on the quality of structures produced by wire arc additive manufacturing (WAAM) using the CMT method.

MATERIALS

WAAM surfacing tests were conducted on a 150×60×8 mm flat bar substrate made of rolled 304 austenitic steel. The 316LSi steel was used as an additional material in the form of a 0.8 mm diameter wire for the production of sample walls. Table 1 shows the chemical composition of 316LSi steel, taken from manufacturer's datasheets. The 316LSi wire is a commercial welding wire used for welding stainless steels that contain molybdenum. The addition of silicon improves weldability by increasing the fluidity of the liquid metal. The chemical composition of the deposit and the 304 steel substrate was measured in

Table 1. Chemical composition of 304, 316LSi steels used in the experiment of WAAM deposition and measured composition of produced deposits

	C	Mn	Si	P	S	Cr	Ni	Mo	N	Cu	Fe
304	0.03	2.01	0.37	0.03	0.01	18.32	8.13	0.29	0.04	0.25	bal.
316LSi	Max. 0.025	1.8	0.9	-	-	18.5	12.5	2.6	-	Max. 0.2	bal.
Deposit	0.043	1.65	0.880	0.024	0.015	17.98	12.27	2.59	0.04	0.112	bal.

layers 16 and 17 using a Belec IN-SPECT stationary spectrometer. Vertical thin walls were produced using a robotic station consisting of a 5-axis IRP-6 robot manufactured by ZAP-Robotyka and a CMT welding machine TPS 2700 Fronius (Figure 1).

The wall samples produced using the WAAM CMT method were 120 mm long and comprised of 24 layers. The welding process involved reciprocating movement of the CMT gun holder. After completing one layer, the gun returned along the same path (Figure 2). This movement strategy limited large deformation or collapse of the walls in the areas where the arc was struck, specifically at the end and beginning of each layer of the wall being built. Moreover, each subsequent layer deposition began only when the temperature of previous layer dropped to 100°C (monitored using UNI-T UTI260B pyrometer). This technique minimizes heat accumulation in the deposited layers. If a subsequent layer is deposited on a surface with a low enough temperature, a steady state deposition can be maintained, resulting in a fixed weld pool size [30]. A similar effect can be achieved by using a pause time between the beads. During the deposition process, heat is transferred to the substrate and is rapidly dissipated. Heat accumulation increases as the deposited thickness increases, reducing the rate at which heat dissipates [33].

To prevent deformations caused by welding stresses during wire deposition, the base material was secured to a rigid plate using fastening devices. This prevents any deformation of the welded plate and wall, which could cause the length of the electrode extension to change as subsequent layers become deposited. During automated layer deposition by WAAM, it is crucial to constantly monitor the position of the welding gun relative to the object being manufactured. In welding tests, the length of the electrode extension was controlled using a plate standard of appropriate thickness. The measurement and correction, if necessary, were made every two layers, always at the same end of the built deposit, to ensure the shape of the reference surface from which the measurement was taken remained constant. The height of the sample varies along its length, therefore the
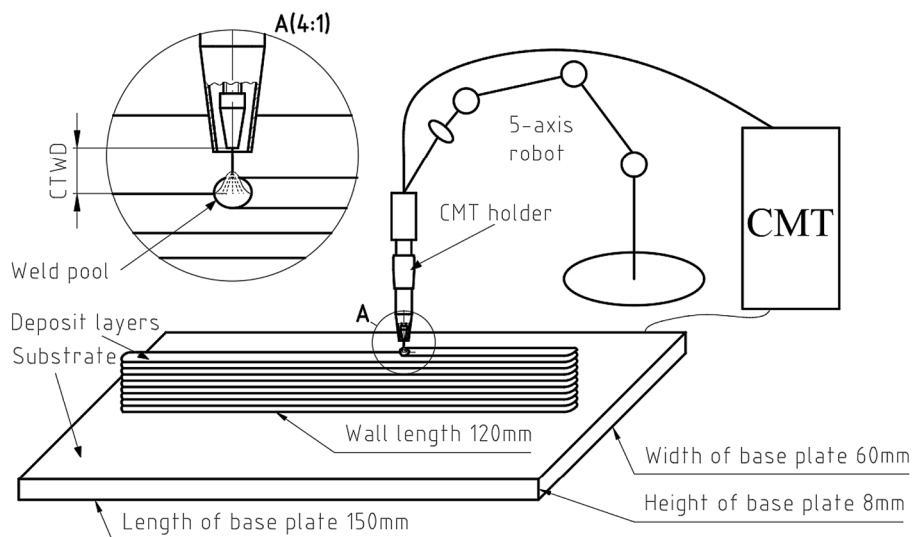

Figure 1. Schematic of a workbench for additive manufacturing of samples in the shape of thin vertical walls with CMT welding machine
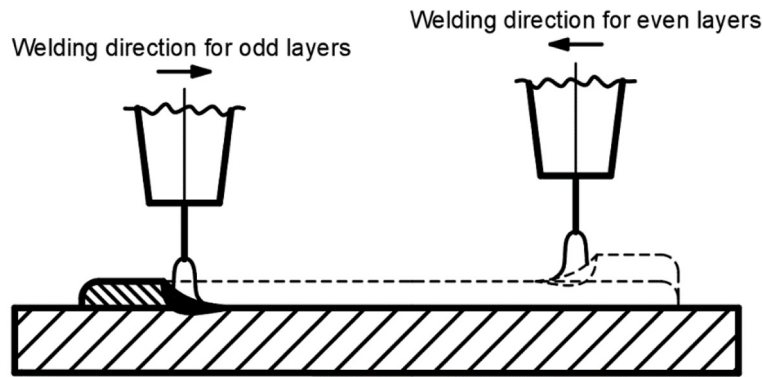
Figure 2. The movement strategy used in WAAM manufacturing of thin wall samples

gas nozzle to work distance (GNWD) value depends on the location of measurement. Twelve additive deposition tests were conducted using three different lengths of contact tip to work distance (CTWD): 10 mm (sample 1), 16 mm (sample 2), and 24 mm (sample 3). To ensure process repeatability, four deposition tests were performed for each set of parameters. The remaining process parameters, as shown in Table 2, were kept constant for each trial.

Samples taken from each model are shown in Figure 4. Although the same process parameters were used to calculate the heat input and the same number of layers were used, the height of the produced structures varies.
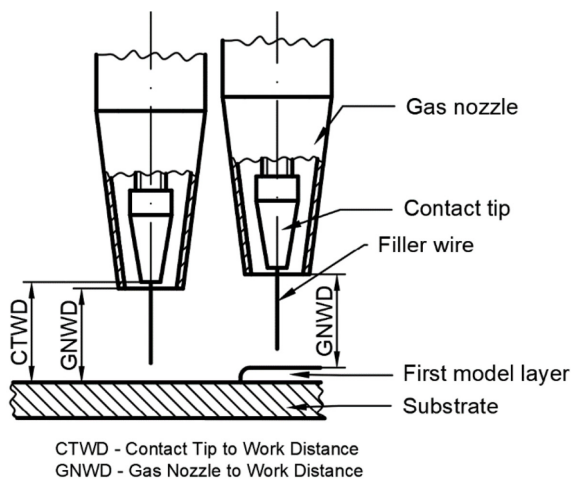
GEOMETRY AND MACROSTRUCTURE CHARACTERIZATION

The initial stage of the research involved non-destructive testing of sample surfaces immediately after the WAAM process. The ATOS Compact Scan 5M device was used to obtain digital models of the samples through 3D laser scanning. The obtained models were processed and analyzed in
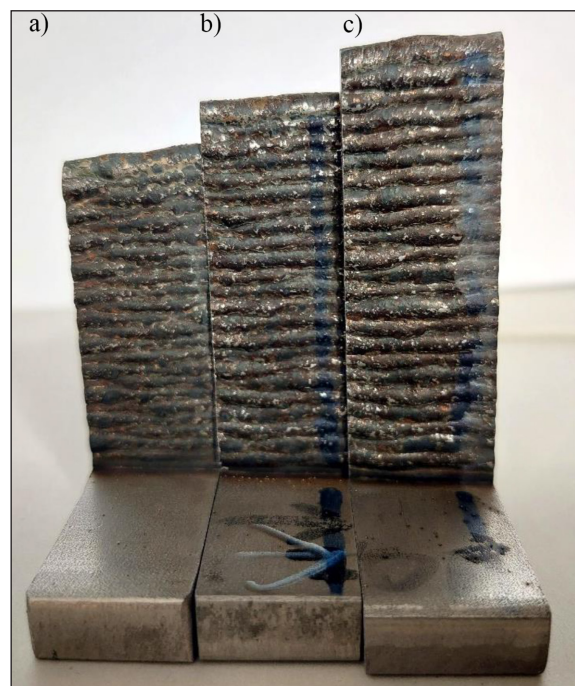

Figure 3. The GNWD distance correction measurement scheme carried out prior to every second layer

Figure 4. Cut out wall fragments made with different CTWD values: (a) CTWD= 10 mm, (b) CTWD=16 mm, and (c) CTWD=24 mm

Table 2. The WAAM CMT incremental deposition parameters used in the tests

Welding current [A]	Arc voltage [V]	Travel speed [mm/s]	Shielding gas flow rate [l/min]	Type of shielding gas	Maximal interpass temperature [°C]	Filler wire feed rate [m/min]
70	13.3	6.75	15	Ar+2%O$_2$	100	6.2

the GOM Inspect program. To perform a surface analysis, a reference model must be defined. For this study, one of the scans from a given series of samples was selected as the reference model. Geometric tests were performed on the entire surface of the deposited layers. We analyzed both models manufactured with the same parameters and conditions, as well as models manufactured with different electrode extensions.

Figure 5 shows the results of the comparative analysis of WAAM models (fitting maps). The series of photos in Figure 5 allows for the assessment of the repeatability of the WAAM process under specific conditions. Sample 2 with CTWD=16 mm was chosen as the reference geometry as this

length is commonly used in literature. The maps were created by overlaying the remaining sample models onto the reference model and calculating the fitting deviation. This deviation represents the difference in coordinates between a given point in the model and its corresponding closest point in the reference model.

Figure 5 presents a comparison of three samples made with different CTWD values, 10 mm, 16 mm, and 24 mm. Samples 1 and 3 were compared to sample 2. The images in Figure 5 are created by applying a deviation map to the reference geometry of sample 2. To enhance graphic readability, we assign colours to difference values that are consistent with the attached legend. The range
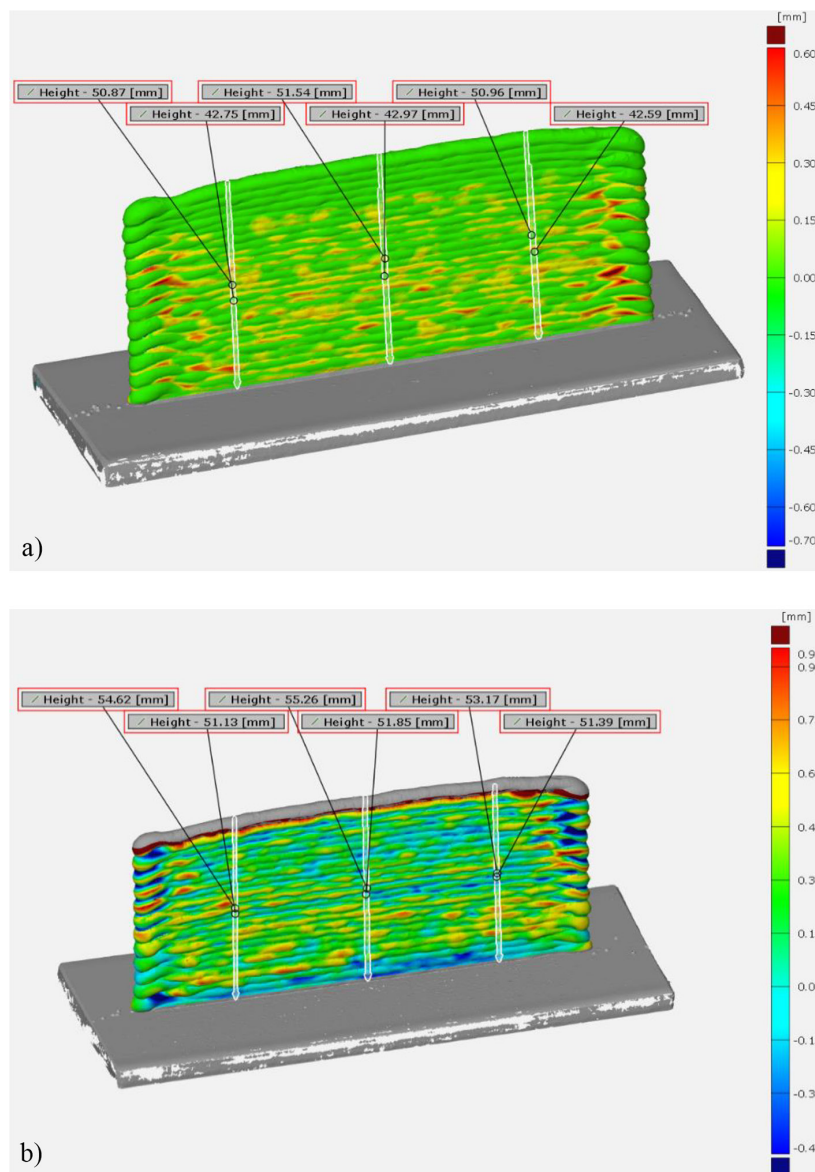

Figure 5. Comparison of sample geometries: (a) sample 1 (CTWD = 10 mm) with sample 2 (CTWD = 16 mm); (b) sample 2 (CTWD = 16 mm) with sample 3 (CTWD = 24 mm)

we have adopted allows for the visualisation of over 95% of the data (deviation values included). However, this means that a small portion of the results is excluded from the analysis, which would otherwise widen the ranges of data values in the legend and reduce the resolution of the results.

Upon examining the deviation maps, it is evident that the colour green is predominant, particularly in Figure 5a. This indicates that, for the majority of the observed surface, the deviation from the reference sample surface is within the range of ±0.15 mm. In a few instances, the colour red appears, indicating areas where the surface mismatch is less than 0.45 mm. Figure 5b shows greater deviation values when comparing samples 2 and 3. The discrepancy between the samples increases and negative values appear, indicating that in certain areas the thickness of sample 3 is less than the thickness of sample 2.

Special attention should be given to the negative deviation value as elements produced using the WAAM method often require additional machining. The ability to produce a sample with a lower thickness may require the production of samples with greater wall thicknesses, reducing the economics of production.

Samples produced using the WAAM method have a layered structure with distinct individual beads. Altering the dimensions, such as the height

of one bead, would cause a direct shift in the position of the remaining beads, potentially resulting in an almost linear indication. The surface profile would be wavy and periodic. The comparison result can be caused by the largest width dimension of one sample overlapping with the smallest width dimension of the reference sample.

Upon comparing the geometries of samples 2 and 3 (Figure 5b), it is evident that there are several areas distributed throughout the sample surface with a mismatch greater than 0.3 mm. Only a few areas of the samples exhibit a deviation greater than 0.6 mm. These deviations are particularly likely to occur at the beginning and end of each bead, which are the places of arc ignition and extinction. The remaining areas with deviations above 0.6 mm are randomly distributed on the sample surface.

Sample 1 has smaller deviations from the reference model (sample 2), as shown in Figure 5a. Increasing the CTWD value from 10 to 16 mm causes less change in the surface's geometric structure than increasing it from 16 to 24 mm. CTWD values greater than 15–16 mm are rarely used in welding processes. The effectiveness of the arc gas shield changes as the CTWD changes. Insufficient shielding can have an effect on the stability of the arc burn and the transfer of the metal, leading to a reduction in the quality of the
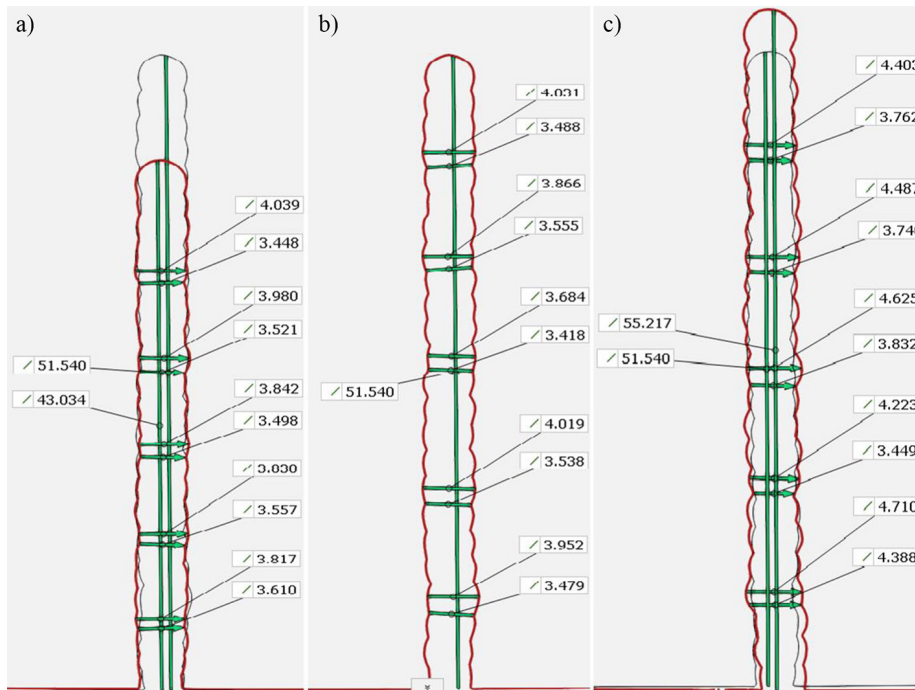

Figure 6. The influence of the length of the electrode extension (CTWD) on the change in the geometry of the sample cross-section: (a) CTWD = 10 mm, (b) CTWD = 16 mm, (c) CTWD = 24 mm

surface. It is important to note that when using a 0.8 mm diameter welding filler wire for WAAM deposition, it may not be stiff enough at higher CTWD values, causing the tip to deflect and affecting the ability to follow the planned movement trajectory.

The geometry of samples made with different values of the electrode extension was analysed in the next stage. Data for comparison were obtained through scanning. Cross-sections were made from 3D models located halfway along the model's length. Height and thickness measurements were taken on these cross-sections. Thickness measurements were taken at the height of layers No. 4, 8, 12, 16, and 20. Measurements were taken at the widest and narrowest points of each layer due to the wavy shape of the side surface of the weld deposit. Figure 6 shows the outline of the shape of multi-layer deposits made with different values of electrode extension. To better visualize the differences in the geometry of the samples, the outline of the analyzed layer and the reference sample (CTWD=16 mm) are shown in red in Figures 6a and 6c.

Figure 6 shows that altering the length of the electrode extension affects the weld geometry. The model created with CTWD = 10 mm is 42.77 mm tall. As CTWD increases, so does the model height, with the CTWD = 16 mm variant reaching 51.15 mm and the CTWD = 24 mm variant reaching 54.6 mm. Changing the CTWD parameter from 10 to 16 mm did not significantly affect the wall thickness. The average value remained approximately 3.7 mm (Table 3). However, increasing the CTWD value to 24 mm resulted in a thicker layer of 4.16 mm (Table 3). The average sample thickness and height, along with their standard deviation, were calculated using data from ten and five measurements of the samples, respectively, as shown in Table 3.

The oval shape of the bead cross-section makes it impossible to achieve uniform wall thickness at all cross-section heights. Figure 7 shows that the wall thickness for samples 1 and 2 follow a similar pattern. Increasing the electrode extension from 10 mm to 16 mm increased the bead height while maintaining its width. For sample 2 (CTWD = 16 mm), the standard deviation for thickness remains at a similar level to that of sample 1 (CTWD = 10 mm). This suggests that the welding conditions are stable. Increasing CTWD to 24 mm resulted in a taller model with wider beads on average, but also increased the standard deviation, making this variant the least repeatable. Furthermore, although the maximum interpass temperature was maintained at around 100°C, the average wall thickness of the model increased, which was not observed in samples made with a lower CTWD value.

The increase in bead volume is caused by the longer electrode extension, which increases the electrical resistance of the circuit. This in turn increases the temperature of the filler wire and speeds up the melting process. To maintain a constant arc length and voltage, the welding machine controller increases the filler metal feeding speed, resulting in a larger deposit layer. An increase in the standard deviation of the layer thickness may be caused by a decrease in the stability of the wire tip guidance, which occurs as CTWD increases. In addition, increasing the CTWD causes the resistance of the electrode wire end to change, resulting in slight penetration and a steeply crowned weld bead geometry in the deposited layer [34].

The use of a short arc in the WAAM process may reduce the energy input into the material, which has an impact on the geometric properties of the resulting products, such as height and wall thickness. Studies on low alloy steels have shown that adjusting the CTWD value can reduce the unit energy in the welding process by up to 40%, which also affects the microstructural properties of the material [35].

Roughness and waviness

The next stage of the research was to characterise the condition of the side surface of the manufactured walls. To measure the surface roughness

Table 3. Geometry wall measurements for different values of contact tip to work distance

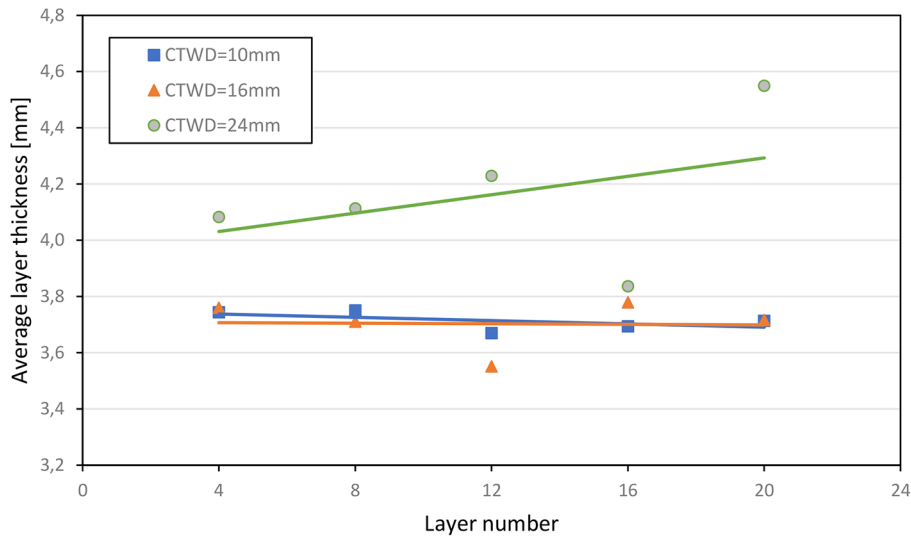| CTWD (mm)	10	16	24
Average sample thickness (mm)	3.71	3.70	4.16
Standard deviation of sample thickness (mm)	0.24	0.21	0.43
Average sample height (mm)	42.77	51.15	54.60
Standard deviation of sample height (mm)	0.14	0.23	0.74

Figure 7. The change in average bead thickness based on the measurement location

and waviness parameters, an optical profilometer VEECO NT2000 was used. The tests were local in nature due to the small measuring field of the profilometer. Figure 8 shows the 3D profilogram created by assembling several smaller parts.

The movement strategy of the CMT gun and the wall shape of the model caused defects in the form of thickenings at the ends of the model, which were not measured. Profilograms were taken in areas where WAAM deposition conditions were stable, resulting in a more uniform geometry. Figure 8 shows an example of roughness measurement results for sample 3 (CTWD = 24 mm). The surface exhibits high waviness and

heterogeneity. The location of the 2D profilogram plot (along the line) affects parameters such as waviness or roughness. The short wave deviation (plotted on the profile of a wavy surface) is an appropriate roughness parameter for the characterisation of the entire surface of the model. Upon observing samples produced using the WAAM method, it is evident that they possess a surface profile that repeats periodically. This surface defect is typical of WAAM additive manufacturing and cannot be avoided, but process optimization can help to limit shape deviations.

The measurements were taken in two directions: the increase in model height and the
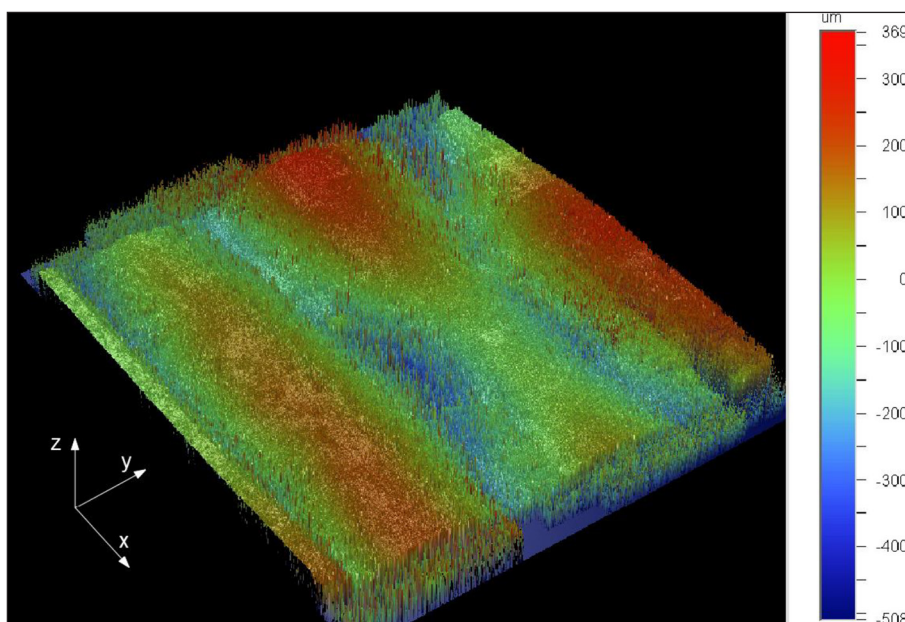

Figure 8. 3D profilograms of surface condition measurement results for sample 3 (CTWD = 24 mm)

direction of surfacing (deposition). Figures 9–11 show profilograms along the measurement lines, and Table 4 presents the results of roughness measurements for the analyzed samples.

The profilograms in Figures 9 to 11 show abrupt changes in roughness parameters for individual samples and measurement directions. These changes can affect the calculated values of surface parameters. However, the limited sensitivity of roughness parameters, i.e. Ra and Rq, means that these parameters only show certain trends well due to their random occurrence. The roughness value obtained is generally lower when measurements are taken in the X direction (along the beads), indicating that the direction of measurement has an impact on the results.

Lower surface sample roughness was achieved with a smaller electrode extension, regardless of the measurement direction. Sample 1, made with the smallest electrode extension, was most affected by the measurement direction. As the CTWD increased, the roughness differences between measurement directions decreased. The obtained Ra value of 20 μm for sample 1 falls within the typical range for cast products.

The changes in the geometric structure of the surface should be analysed separately for surface waviness and roughness. Changes in surface waviness resulting from the WAAM process are caused by changes in the volume of the bead. The higher the linear energy (and wire feed speed), the larger the bead dimensions and the greater the surface waviness. Roughness is a parameter that measures irregularities with relatively small peak distances. In Figure 11, the profilogram shows many roughness values in the area marked with a frame. This parameter is less dependent on the thermal parameters of the deposition process that affect waviness. The changes observed in roughness at the surface layer may have been influenced by the deterioration of gas shielding conditions with the increase in CTWD. Insufficient shielding can lead to excessive oxidation of the metal while it is still hot, which can affect the condition of the surface layer.

Microstructure characterization

Samples were obtained from the cut wall models for microstructural tests to demonstrate the cross-section of the layers. The testing samples
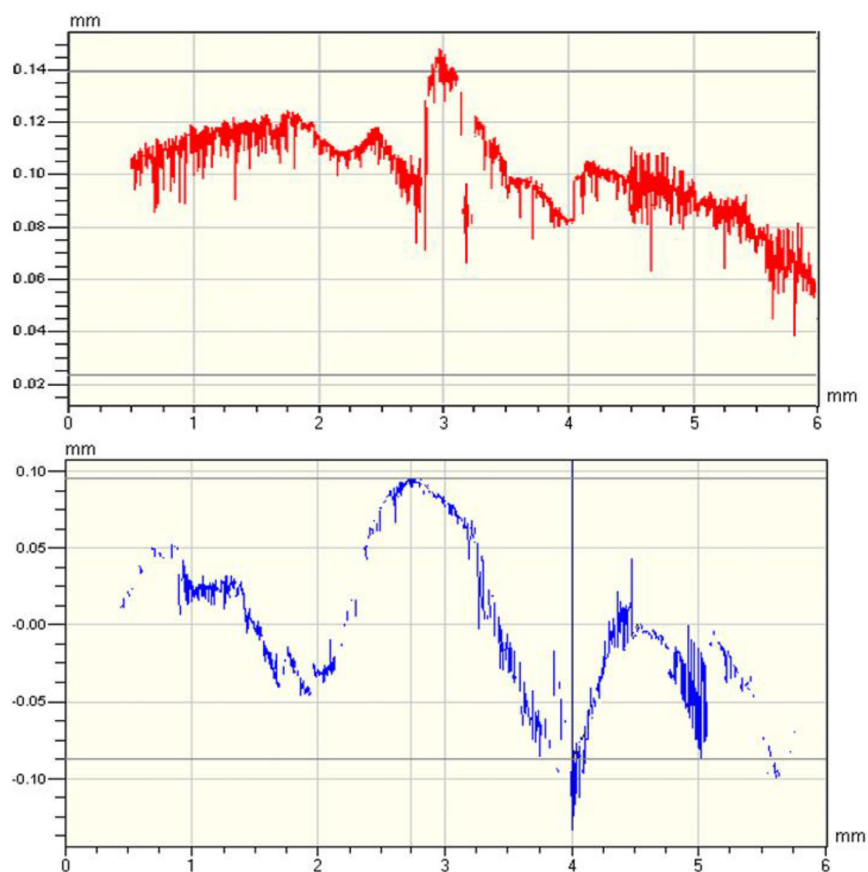

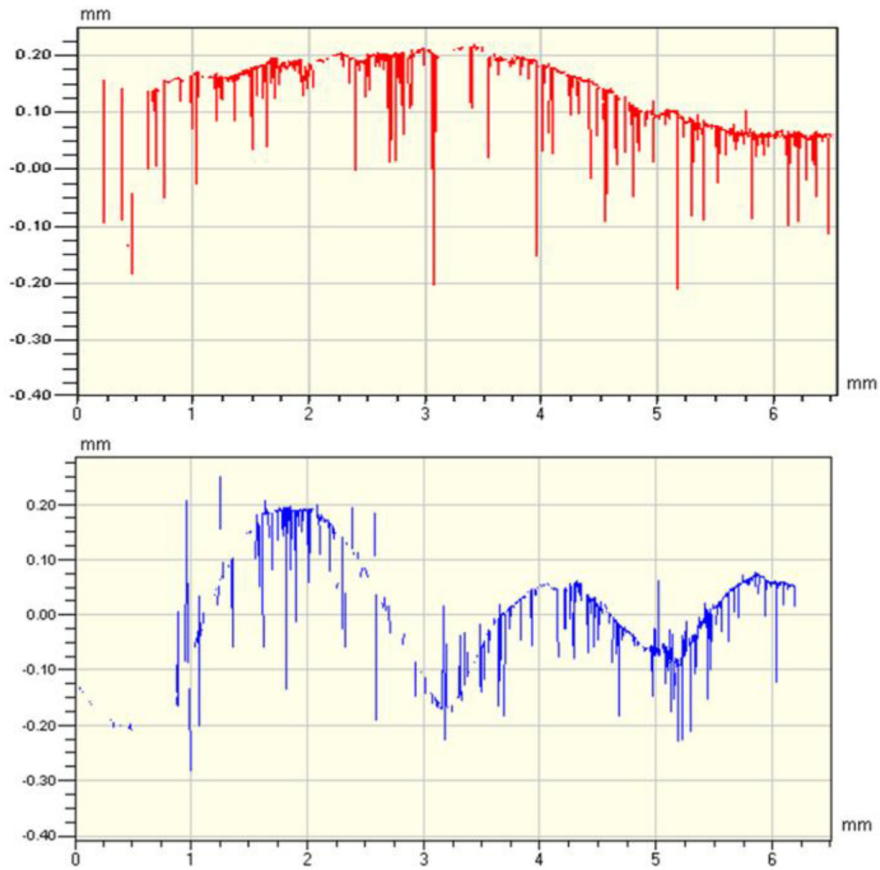**Figure 9.** Roughness profiles measured in X (top) and Y (bottom) direction for CTWD = 10 mm

Figure 10. Roughness profiles measured in X (top) and Y (bottom) direction for CTWD = 16 mm
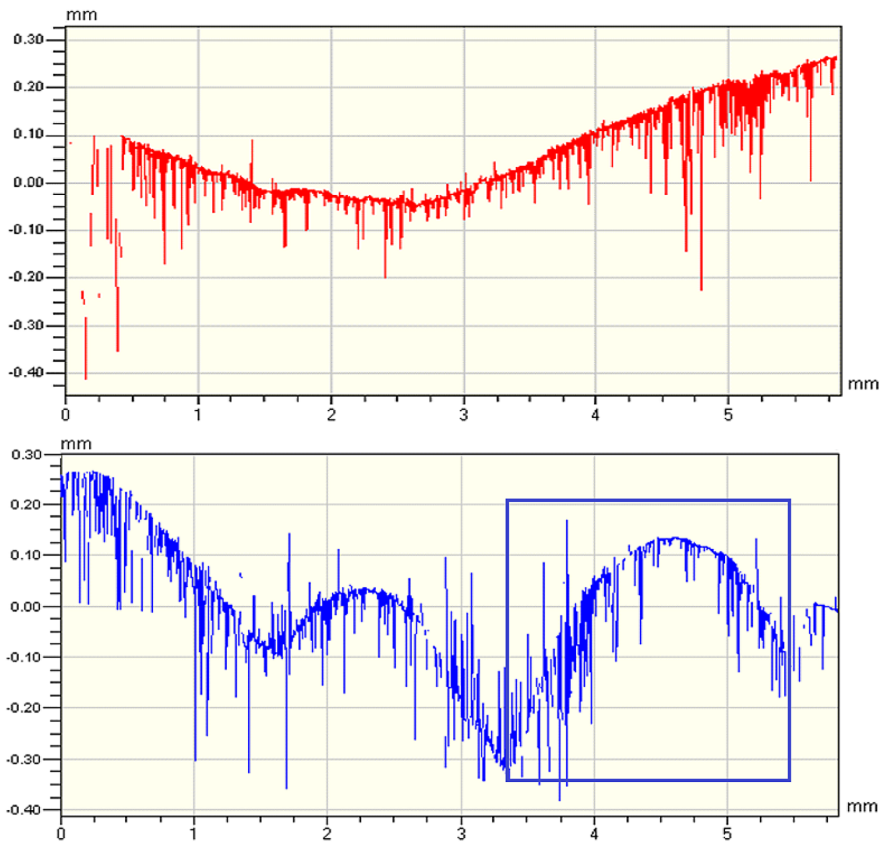

Figure 11. Roughness profiles measured in X (top) and Y (bottom) direction for CTWD = 24 mm

Table 4. Roughness parameters for two measurement directions of analyzed samples

Roughness (µm)	CTWD = 10 mm		CTWD = 16 mm		CTWD = 24 mm	
	Measurement direction					
	X	Y	X	Y	X	Y
Ra	20	60	60	80	90	100
Rt	120	230	590	630	700	650
Rq	20	60	70	100	110	130
Rp	150	100	220	250	290	270

were taken 25 mm away from the model's edge. Metallographic specimens were prepared by grinding the cut pieces on a metallographic grinder-polisher. The grinding process began with P100 grit sandpaper and ended with P2500. Alumina (Al_2O_3) was used as an abrasive to polish the samples. The polished surfaces were then etched with a solution of copper chloride ($CuCl_2$) and hydrochloric acid (HCl) in water. Figure 12 shows the macrostructure of the samples.

The samples were examined at both the macroscopic and microscopic levels. Macroscopic examination was carried out using an Olympus SZ61 stereoscopic microscope with 6.67x magnification. Due to the magnification used, it was not possible to cover the entire sample in one image, so a series of photographs were taken and assembled in a graphic editor. Microscopic examinations were conducted using an Olympus BX51M reflected light microscope at magnifications of 50, 100, and 200 times. The research focused on specific areas of the observed structure, including the upper part of the last layer, the side edges of the beads, and the areas between the beads (fusion zones). Photographic documentation was created using Olympus Stream Essential software.

Figure 13a and b display the upper surface of the final layer. The matrix, which is the dominant phase, consists of austenite (bright phase visible in the photos), while ferrite phase is distributed along the boundaries of the austenite grains. The unique characteristic of this layer is its distinct structural morphology. In the lower part of Figure 13, large, highly oriented, and parallel columnar crystals are visible. Just below the surface, the structure loses its orientation and takes on a dendritic shape, with dendrites containing a greater proportion of the dark phase. This change may be due to alterations in the heat dissipation mechanisms within the layer. The top layer dissipates heat by conduction to the centre and by radiation and convection to the surroundings.

Crystallisation is faster in this layer, leading to the formation of dendrites with different orientations. Figure 14 shows a similar structure, possibly due to different heat dissipation conditions at the surface compared to the volume of the material, near the side edges of each layer. Furthermore, the upper section of the final layer does not experience the heat treatment effects caused by the thermal cycle induced by another bead. Figures 13-16 display pairs of photos that depict similar parts of the sample's cross-sectional structure.
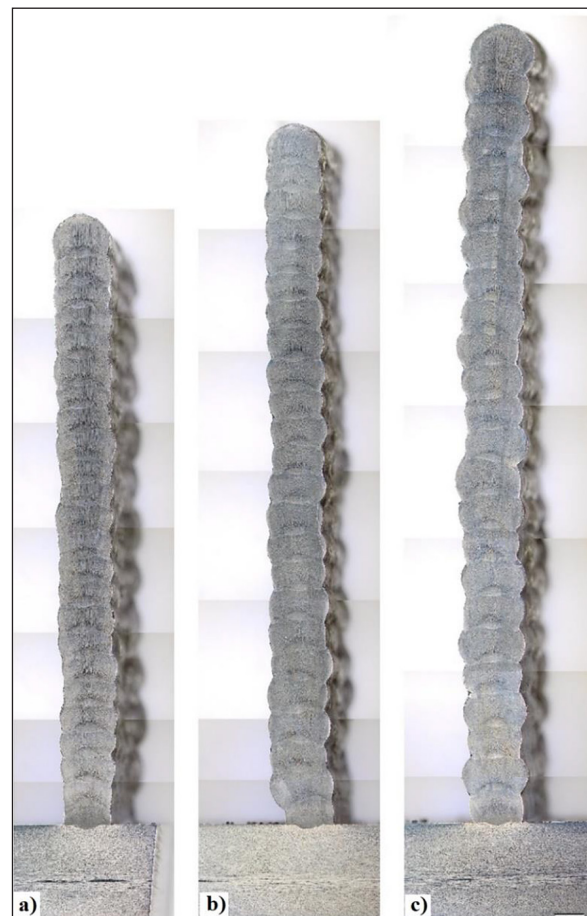

Figure 12. Cross-section of a sample produced by WAAM CMT method: (a) CTWD = 10 mm, (b) CTWD = 16 mm, (c) CTWD = 24 mm
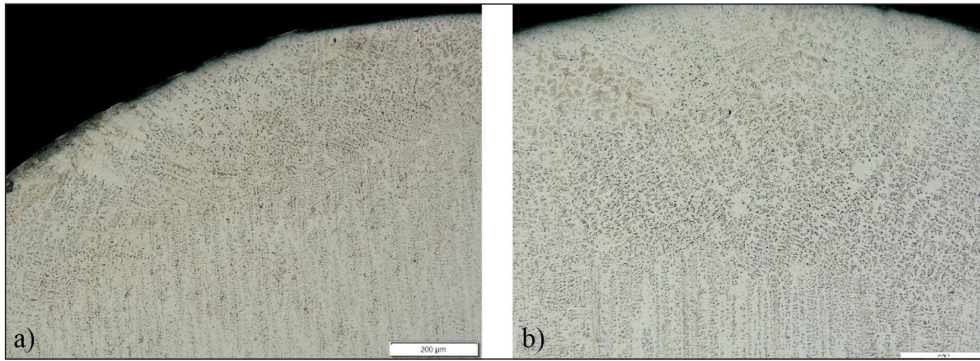
Figure 13. Microstructure of the upper part of the last layer: (a) in the sample 3 (CTWD = 24 mm), (b) in the sample 1 (CTWD = 10 mm)
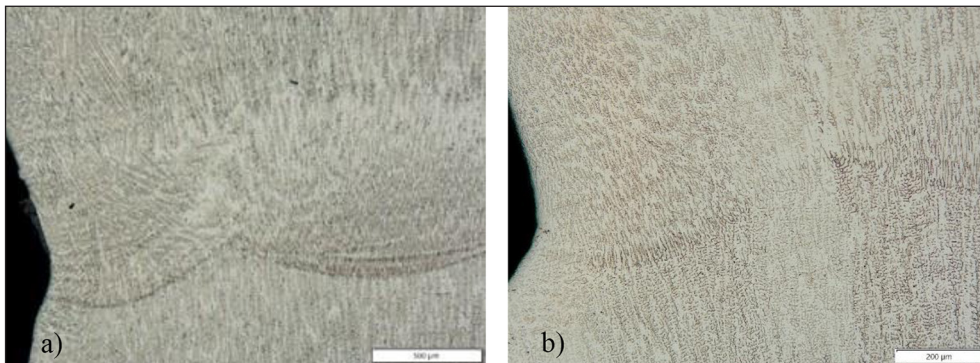

Figure 14. Microstructure: (a) in the sample 2 (CTWD = 16 mm), at the interface between 15 and 16th layer, (b) in the sample 3 (CTWD = 24 mm), at the interface between 4 and 5th layer
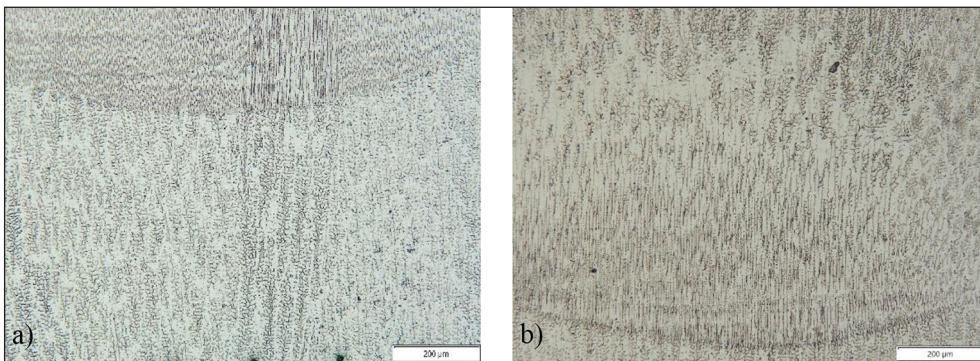

Figure 15. Microstructure: (a) in the sample 1 (CTWD = 10 mm) at the fusion line between 6 and 7th layer, (b) in the sample 2 (CTWD = 16 mm), at the interface between 15 and 16th layer

Figures 14–16 display the area where two adjacent beads meet, marked with a fusion line. The columnar structure in the lower layer is continuous and remains almost unchanged in the next layer, as shown in Figure 12.

Figure 15a illustrates the columnar structure of the grains, which is preserved during the transition from the lower to the upper layer (epitaxial grain growth). The morphology of the ferrite in the austenite matrix has changed within the column. The changes in the structure are noticeable from the fusion line upwards. Behind the fusion line, the previously dendritic, two-dimensional vermicular ferrite precipitates change to quasi one-dimensional, columnar ferrite that is vertically oriented (see Figure 16). Following this, an area with fewer dark precipitates is observed (upper part of Figure 15b), before returning to the
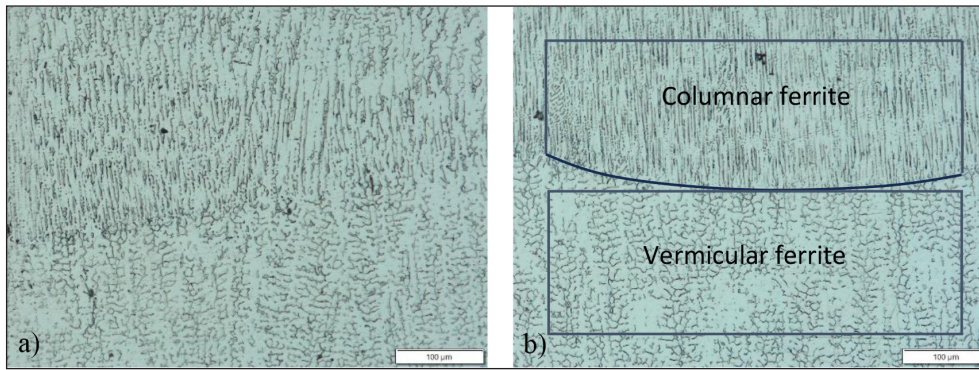
Figure 16. Microstructure: (a) in the sample 2 (CTWD = 16 mm) at the fusion line between 6 and 7th layer, (b) in the sample 1 (CTWD = 10 mm) at the fusion line between 15 and 16th layer

same structure as below the fusion line. These changes occur in each layer independently of the process parameters and only affect the dimensions of individual areas of the structures.

Microhardness examination

Microstructural tests were expanded to include microhardness measurements on cross-sections of samples. The microhardness distributions were analysed to assess the impact of electrode extension length on the deposited layer's hardness. Microhardness measurements were taken using a Leitz-Wetzlar tester $\mu HV_{0.2}$ with a 20-second loading time. The distributions in Figure 17 were created to determine the microhardness in the central part of each layer. Four measurements were taken in each layer, and the mean and standard deviation were calculated. Figure 17 shows

that the microhardness distributions have similar patterns. The first two layers exhibit increased hardness, while the courses from the third to the twelfth layer have almost identical microhardness, averaging at approximately 170 $HV_{0.2}$. Samples 2 and 3 show a microhardness of approximately 170 $HV_{0.2}$ from layers 13 to 24, while the microhardness of layers in sample 1 drops to approximately 150 $HV_{0.2}$. Layers 13–24 of the first sample exhibited a slightly lower microhardness, despite controlling the interpass temperature during deposition and using the same process parameters. The microhardness of the structure remains approximately the same in each layer, despite changes in electrode extension, as shown by the quasi-linear microhardness distributions for samples with CTWD=16 mm and CTWD = 24 mm, and partially for sample with CTWD=10 mm.
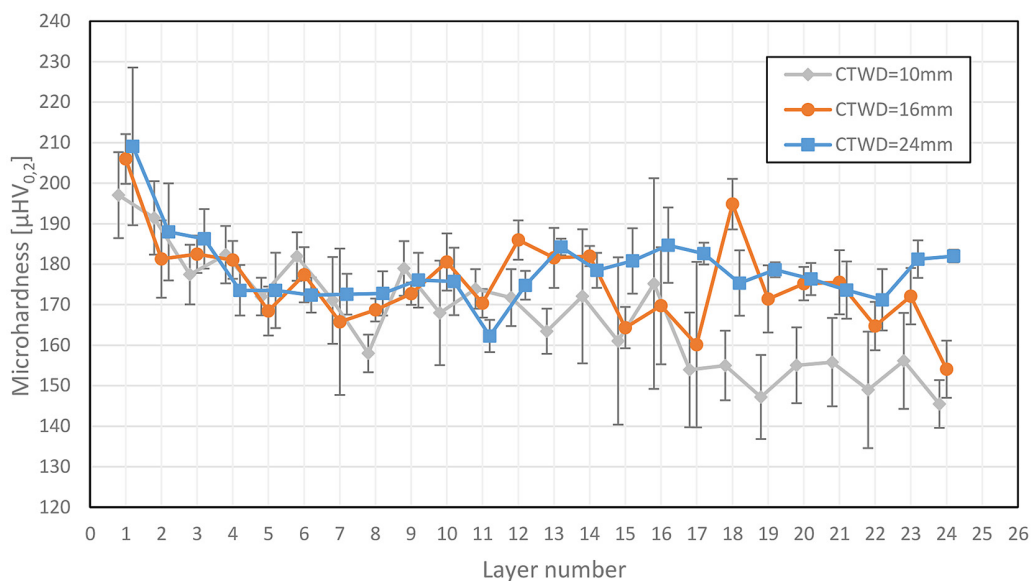

Figure 17. Microhardness distribution on cross-sections of manufactured wall samples

However, there is an increase in microhardness to approximately 200 $HV_{0.2}$ in layers 1 and 2 of all samples. The microhardness of these layers may have increased due to the mixing of the substrate material with filler metal and subsequent rapid cooling. The increase in heat dissipation may be due to the relatively large volume of the cold substrate. It is possible that the rapid cooling has strengthened the material by preventing the diffusion decay of ferrite into austenite, leaving finely dispersed ferrite in the structure and mixing the substrate material with the filler metal. The application of subsequent layers minimizes the impact of the substrate on the layer structure and stabilizes the deposition conditions. According to research [36], the hardness value of the 316L stainless steel sample produced by WAAM decreased gradually from the bottom (~180HV) to the top (~170 HV) due to heat accumulation. However, process parameters such as the transient and gradual reduction of bottom current, scanning speed, and cooling time have little influence on the hardness of the deposited samples.

During the deposition process, heat affects the structure of the underlying layers, but the short exposure time at high temperature means that the effect of multiple thermal cycles on significant changes in microhardness is not observed. Furthermore, when reheated using an electric arc welding heat source, austenitic stainless steels 316L/304 do not undergo a phase transformation that would allow for grain refinement. A small amount of ferrite may form in the area heated to near solidus, but this should not significantly affect the microhardness of the material.

CONCLUSIONS

The study analysed how the length of the electrode extension affects the microstructure, microhardness, and geometry of deposits when using the WAAM method to create straight walls with 316LSi filler wire. Three samples with varying electrode extension values were tested, highlighting the importance of controlling and correcting this parameter during automated production to ensure process repeatability. Based on the research conducted, the following conclusions can be drawn:

- When selecting the parameters for WAAM deposition, it is crucial to include the CTWD parameter. Omitting this parameter can cause uncontrolled changes in the length of the electrode extension, which can affect the thermal conditions of material deposition. This can lead to undesirable and unexpected changes in the layer width and height, making it difficult to ensure repeatable results of WAAM deposition.

- Increasing the CTWD value from 10 mm to 16 mm increased the layer height while maintaining its width. Further increasing the CTWD to 24 mm resulted in an increase in both the thickness and height of the layers.

- The study demonstrated that altering the CTWD value through the use of a synergistic CMT welding machine during WAAM deposition affected the geometry of the produced layers. Increasing the CTWD has a similar effect to increasing the linear welding energy, resulting in an increase in the volume of the deposited layer.

- Using a low CTWD of 10 mm can reduce roughness by enabling stable arc burning with sufficient gas shielding. The roughness values measured on sample 1 (CTWD =10 mm), with Ra=60 μm and Rt=230 μm in the y-direction (perpendicular to the surfacing direction), suggest that a model produced with these parameters could be a semi-finished product comparable to a cast steel semi-finished product with CT tolerance class 8 of the casting. It should be noted that the Rt value has been determined for a measuring section of approximately 6 mm. The total height of the profile over a measuring section equal to the height of the wall may be greater. Depending on its purpose, the surface created for the best variant of the CTWD parameter may require additional mechanical processing, such as when working in a kinematic pair with another surface, or it may be left unprocessed if the surface will not play a significant role, such as being an external part of the bodies or housings. The increase in the roughness expressed by the Ra parameter with the increase in the CTWD value may be caused by the deterioration of the quality of the gas shielding in CMT gun. However, this requires additional verification.

- Microstructural tests indicate that altering the CTWD parameter, while maintaining a controlled interpass temperature, has no significant effect on the microstructure. All examined layers of each sample displayed an almost identical structure. The distribution of the remaining ferrite in the structure is almost identical in each layer. The microstructure of the upper

part of the last layer differed slightly. During the WAAM deposition process with unforced cooling, no mechanism is observed that would significantly increase the microhardness of the samples. No significant increase in microhardness of the samples was observed during the WAAM deposition process with unforced cooling. Reheating the deposited bead using the heat from the next bead can cause a change in grain orientation towards the direction of heat removal. This change may affect the anisotropy of other mechanical properties.

Optimizing the parameters of the WAAM process can lead to models with improved surface quality. However, reducing surface waviness in the direction of model building can be challenging. Lowering the CTWD value and, consequently, reducing the amount of process heat can help reduce surface waviness, but eliminating it completely may prove difficult. In order to achieve this, it is necessary to shape the material while it is still in a liquid state, which can be a technological challenge. The research conducted highlights the significant role of electrode extension in the incremental CMT deposition process.

Acknowledgements

REFERENCES

1. Dilberoglu U.M., Gharehpapagh B., Yaman U., Dolen M. The role of additive manufacturing in the era of Industry 4.0. Procedia Manuf. 2017; 11: 545–554. https://doi.org/10.1016/j.promfg.2017.07.148

2. Prashar G., Vasudev H., Bhuddhi D. Additive manufacturing: expanding 3D printing horizon in industry 4.0. Int. J. Interact. Des. Manuf. 2022. https://doi.org/10.1007/s12008-022-00956-4.

3. Gibson I., Rosen D.W., Stucker Br. Additive Manufacturing Technologies Rapid Prototyping to Direct Digital Manufacturing. Springer New York, 2015. https://doi.org/10.1007/978-1-4419-1120-9.

4. Gade S., Vagge S., Rathod M. A review on additive manufacturing – methods, materials, and its associated failures. Advances in Science and Technology Research Journal 2023; 17(3): 40–63. https://doi.org/10.12913/22998624/163001

5. Ananda P.A., WAAM Application for EPC Company,

6. Kah P. Advancements in Intelligent Gas Metal Arc Welding Systems Fundamentals and Applications. Woodhead Publishing Series in Welding and Other Joining Technologies, 2021; 1-103. Elsevier Science Ltd. https://doi.org/10.1016/C2019-0-04191-X

7. Guo N., Leu M.C. Additive manufacturing: technology, applications and research needs. Front. Mech. Eng. 2013; 8: 215–243. https://doi.org/10.1007/s11465-013-0248-8

8. Kołodziejczak P., Bober M., Chmielewski T. Wear Resistance Comparison Research of High-Alloy Protective Coatings for Power Industry Prepared by Means of CMT Cladding. Applied Sciences, 2022; 12(9): 4568, 1-13. https://doi.org/10.3390/app12094568

9. Chen X., Su C., Wang Y. et al. Cold Metal Transfer (CMT) Based Wire and Arc Additive Manufacture (WAAM) System. J. Surf. Investig. 2018; 12: 1278–1284. https://doi.org/10.1134/S102745101901004X

10. Naidu D.S., Ozcelik S., Moore K.L. Modeling, Sensing and Control of Gas Metal Arc Welding, Elsevier Science Ltd, 2003. https://doi.org/10.1016/B978-0-08-044066-8.X5000-9

11. Li Y., Su, C. Zhu J., Comprehensive review of wire arc additive manufacturing: Hardware system, physical process, monitoring, property characterization, application and future prospects, Results Eng. 2022; 13: 100330. https://doi.org/10.1016/j.rineng.2021.100330

12. Bintao W. A review of the wire arc additive manufacturing of metals: properties, defects and quality improvement. J. Manuf. Processes. 2018; 35: 127-139. https://doi.org/10.1016/j.jmapro.2018.08.001.

13. Salmi, M. Pei E. Additive manufacturing processes and materials for spare parts. J. Mech. Sci. Technol. 2023; 37(11): 5979-5990. https://doi.org/10.1007/s12206-023-1034-0

14. Williams S.W., Martina F., Addison A.C., Ding J., Pardal G., Colegrove P. Wire + Arc Additive Manufacturing, Materials Science and Technology, 2016; 32(7): 641-647. https://doi.org/10.1179/1743284715Y.0000000073

15. Taşdemir A., Nohut S. An overview of wire arc additive manufacturing (WAAM) in shipbuilding industry, Ships and Offshore Structures, 2021; 16(7): 797-814. https://doi.org/10.1080/17445302.2020.1786232.

16. Wordofa T.N., Ramulu, P.J. Gas Metal Arc Welding Input Parameters Impacts on Weld Quality Characteristics of Steel Materials a Comprehensive Exploration. Manuf. Technology, 2023; 3(23): 366-379. https://doi.org/10.21062/mft.2023.046

17. Silva R.H.G., dos Santos Paes L.E., Barbosa R.C. et al. Assessing the effects of solid wire electrode

MATEC Web of Conferences 269, 05002 (2019), https://doi.org/10.1051/matecconf/201926905002

extension (stick out) increase in MIG/MAG welding. J Braz. Soc. Mech. Sci. Eng. 2018; 40: 31. https://doi.org/10.1007/s40430-017-0948-9

18. Shen H., Deng R., Liu B., Tang S., Li S. Study of the Mechanism of a Stable Deposited Height During GMAW-Based Additive Manufacturing. Appl. Sci. 2020; 10: 4322. https://doi.org/10.3390/app10124322

19. Cicic D.T., Rontescu C., Amza C.G., Semenescu A. Research Concerning the Influence of Contact Tip-to-Work Distance (CTWD) on Penetration, Bead Height, Bead Width - Study Case GMAW Cladding. AMR 2015, 1088,774–8. https://doi.org/10.4028/www.scientific.net/amr.1088.774

20. Ali M.H., Han Y.S. A Finite Element Analysis on the Effect of Scanning Pattern and Energy on Residual Stress and Deformation in Wire Arc Additive Manufacturing of EH36 Steel. Materials, 2023; 16: 4698. https://doi.org/10.3390/ma16134698

21. Marefat F., Kapil A., Banaee S.A.,Van Rymenant P., Sharma A. Evaluating shielding gas-filler wire interaction in bi-metallic WAAM of creep resistant steel-stainless steel for improved process stability and build quality. J. Manuf. Processes. 2023; 88: 110–124. https://doi.org/10.1016/j.jmapro.2023.01.046

22. Kemény D.M., Sándor B., Varbai B., Katula L.T., The effect of arc voltage and shielding gas type on the microstructure of wire arc additively manufactured 2209 Duplex stainless steel, Advances in Materials Science, 2033; 23: 4(78). https://doi.org/10.2478/adms-2023-0023

23. Ghumman K.Z., Ali S., Ud Din E., Mubashar A., Khan N.B., Ahmed S.W. Experimental investigation of effect of welding parameters on surface roughness, micro-hardness and tensile strength of AISI 316L stainless steel welded joints using 308L filler material by TIG welding, J. Manuf. Res. Technol. 2022; 21: 220-236. https://doi.org/10.1016/j.jmrt.2022.09.016

24. Xiong J., Li Y., Li R., Yin Z. Influences of process parameters on surface roughness of multi-layer single-pass thin-walled parts in GMAW-based additive manufacturing, J. Mater. Proc. Technol., 2018; 252: 128-136. https://doi.org/10.1016/j.jmatprotec.2017.09.020

25. Nagasai B.P., Malarvizhi S., Balasubramanian V. Mechanical properties and microstructural characteristics of wire arc additive manufactured 308 L stainless steel cylindrical components made by gas metal arc and cold metal transfer arc welding processes, J. Mater. Proc. Technol. 2022; 307: 117655. https://doi.org/10.1016/j.jmatprotec.2022.117655

26. Belotti L.P , van Nuland T.F.W., Geers M.G.D., Hoefnagels J.P.M., van Dommelen J.A.W. On the anisotropy of thick-walled wire arc additively manufactured stainless steel parts, Mater. Sci. Eng. 2023; A863: 144538. https://doi.org/10.1016/j.msea.2022.144538

27. Bruggi M., Laghi V., Trombetti T. Optimal Design of Wire-and-Arc Additively Manufactured I-Beams for Prescribed Deflection, Comput. Assisted Methods Eng. Sci. 2022; 29(4): 357–378. https://doi.org/10.24423/cames.469.

28. Zhou T., Zheng T., Yildiz A.B., Spartacus G., Rolinska M., Cubitt R., Hedstrom P. Microstructure control during deposition and post-treatment to optimize mechanical properties of wire-arc additively manufactured 17-4 PH stainless steel. Addit. Manuf. 2022; 58: 103047. https://doi.org/10.1016/j.addma.2022.103047.

29. Wahsh L.M., El Shater A.E., Mansour A.E., Hamdy F.A., Turky M.A., Azzam M.O., Salem H.G. Parameter Selection for Wire Arc Additive Manufacturing (WAAM) Process, Contributed Papers from Materials Science and Technology 2018 (MS&T18) October 14–18, 2018, Columbus, Ohio, USA, 78-85. 10.7449/2018mst/2018/mst_2018_78_85.

30. Rodrigues T.A., Duarte V., Avila J.A., Santos T.G., Miranda R.M., Oliveira J.P. Wire and arc additive manufacturing of HSLA steel: Effect of thermal cycles on microstructure and mechanical properties. Addit. Manuf. 2019; 27: 440-450. https://doi.org/10.1016/j.addma.2019.03.029.

31. Suarez A., Aldalur E., Veiga F., Artaza T., Tabernero I., Lamikiz A. Wire arc additive manufacturing of an aeronautic fitting with different metal alloys: From the design to the part. J. Manuf. Proc. 2021; 64: 188–197. https://doi.org/10.1016/j.jmapro.2021.01.012.

32. Cunningham C.R., Flynn J.M., Shokrani A., Dhokia V., Newman S.T. Invited Review Article: Strategies and Processes for High Quality Wire Arc Additive Manufacturing. Addit. Manuf., 2018; 22: 672-686. https://doi.org/10.1016/j.addma.2018.06.020.

33. Lee S.H. CMT-Based Wire Arc Additive Manufacturing Using 316L Stainless Steel: Effect of Heat Accumulation on the Multi-Layer Deposits. Metals. 2020; 10(2): 278. https://doi.org/10.3390/met10020278

34. Shah A., Aliyev R., Zeidler H., Krinke S. A Review of the Recent Developments and Challenges in Wire Arc Additive Manufacturing (WAAM) Process. J. Manuf. Mater. Process. 2023; 7: 97. https://doi.org/10.3390/jmmp7030097

35. Henckell P., Gierth M., Ali Y., Reimann J., Bergmann J.P., Reduction of Energy Input in Wire Arc Additive Manufacturing (WAAM) with Gas Metal Arc Welding (GMAW), Materials, 2020; 13: 2491. https://doi.org/10.3390/ma13112491.

36. Jin W., Zhang C., Jin S., Tian Y., Wellmann D., Liu W. Wire Arc Additive Manufacturing of Stainless Steels: A Review. Applied Sciences. 2020; 10(5): 1563. https://doi.org/10.3390/app10051563